Scenario-based flood adaption of a fast-developing delta city: modeling the extreme compound flood adaptations for Shanghai

Hangxing Wu[a], Min Zhang[a,*], Yi He[b], Peiyan Chen[c], Ulysse Pasquier[b], Hengzhi Hu[d], Jiahong Wen[a]

[a] *School of Environmental and Geographical Sciences, Shanghai Normal University, Shanghai 200234, China*

[b] *Tyndall Centre for Climate Change Research, School of Environmental Sciences, University of East Anglia, Norwich Research Park, Norwich NR4 7TJ, UK*

[c] *Shanghai Typhoon Institute and Laboratory of Typhoon Forecast Technique of China Meteorological Administration, Shanghai 200030*

[d] *Department of Hospitality Management, Shanghai Business School, Shanghai 200234, China*

Corresponding author: Min Zhang, zhangmin@shnu.edu.cn

Abstract

The heavy Zhengzhou "7·20" rainstorm, partially caused by Typhoon In-fa in 2021, poured an unprecedented rainfall of 201.9 mm/h, leading to severe flooding and damage. Although many studies in various Chinese cities have preliminarily assessed the potential flood losses under "7·20" rainstorm, much research has focused on the contribution of climate change, limited attention has been paid to the potential impacts of urbanization development, which is crucial for designing flood adaptation strategies. Using high-resolution ocean-land coupled numerical model, we focus on Shanghai, a fast-developing delta city, to evaluate the potential impact of "7·20" rainstorm associated with local coastal storm hazards for flood adaptation planning under future urbanization scenarios. Our findings reveal that rapid urbanization in Shanghai can significantly amplify flood risks caused by events equivalent to "7·20" rainstorm. By 2050, the projected increases in exposed assets and losses can be up to 8 and 5 times, respectively, if such events occur. The adaptation measure of heightening seawalls and dikes provides robust protection against compound fluvial-coastal flooding events, but is costly and less effective against pluvial flooding. In contrast, low-impact development measures of increasing green area may not offer the highest asset exposure reduction but have low initial costs and provide significant ecological benefits. Lowering green space offers the greatest reduction in exposed assets and losses from pluvial flooding, but it's also costly and may alter the urban landscape. A combination of these measures, where applicable, is recommended to optimize flood resilience and promote sustainable development in rapidly urbanizing delta cities.

Keywords: Zhengzhou "7·20" rainstorm; Coastal adaptation; Rapidly urbanization; Numerical modeling; Delta city

1. Introduction

Fast developing delta cities at low and mid-altitudes are increasingly vulnerable to compound flooding risks driven by rapid urbanization and climate change (Dixon et al., 2006; Tessler et al., 2015). Currently, approximately 500 million people reside in river deltas or nearby areas, where major cities with high population density and significant wealth have developed due to coastal migration (Hugo, 2011) and rapid economic growth (Hallegatte et al., 2013), known as coastal urbanization (Syvitski and Saito, 2007; Chen et al., 2019; Wu et al., 2024). Urgent adaptation actions are needed to protect these cities from escalating compound coastal, fluvial, and pluvial flooding (Jongman, 2018). Slow changes such as sea level rise in the future further exacerbate the vulnerabilities of these low-lying, densely populated coastal areas (Chen et al., 2017; Hanson et al., 2010; Dixon et al., 2006; Syvitski et al., 2009), especially when combined with short-term, devastating events like tropical cyclones and cyclone-induced heavy rainfall (Jongman, 2018; Maymandi et al., 2022). Therefore, it is crucial to investigate the formation and amplification mechanisms of compound flood risk in rapidly developing delta cities to develop effective adaptive measures.

A substantial body of researches have focused on coastal flooding (Hallegatte et al., 2013; Tessler et al., 2015; Vousdoukas et al., 2018; Fang et al., 2020), much of the researches focuses on the hazard drivers, particularly the impacts of future climate change, sea-level rise, and changes in wind and wave intensity (Chen et al., 2017; Hanson et al., 2010; Woodruff et al., 2013; Vitousek et al., 2017). However, studies on the evolving characteristics of disaster-prone environments and the vulnerability of assets that contribute to flood risks remain limited. Recently, there has been increasing attention on land subsidence and its role in exacerbating flood risks (Syvitski et al., 2009; Du et al., 2020; Nicholls et al., 2021; Shirzaei and Bürgmann, 2018). In contrast, research on how land use changes, driven by rapid urbanization, amplify flood risks is still insufficient. Rapid urbanization potentially increases delta flooding risks by altering natural hydrology process and amplifying storm surge damages (Chen et al., 2019; Wu et al., 2024). As cities expand along coastlines, urbanization transforms natural landscapes into impermeable surfaces and disrupts nature water drainage systems (Yang et al., 2022). Additionally, urban sprawl concentrates population and infrastructure, raising the likelihood of extensive damage and human casualties, posing significant challenges for urban planning and disaster risk management (Rimal et al., 2018; Wu et al., 2024).

Data on China's coastal zones indicate that coastal urbanization and population growth amplify flood disaster losses compared to the natural evolutions of flood risks (Chen et al., 2019; Zhang et al., 2021). Moreover, current research on urban flooding in delta city primarily examines flood risk under existing economic conditions (Du et al., 2020; Wang et al., 2019; Chen, 2022). While some studies consider hazard evolution due to climate change, they often overlook the complex amplification of flood risks due to future land-use changes (Wahl et al., 2015; Yang et al., 2022; Wang et al., 2023). Even rarer are studies on modeling flood adaptations for future rapid urbanization (Yang et al., 2022). Flood adaptations for mitigating flood risks under various long-term projections have been explored (Aerts et al., 2014; Du et al., 2020; de Ruig et al., 2019; Yamamoto et al., 2021). However, these studies generally rely on statistical models or basic flooding simulations, lacking the integration of bespoke adaptation solutions into high-precision numerical hydrodynamic models considering urban development. Therefore, an objective model-investigation of detailed flood adaptation designing is significant for reducing compound flood risks in rapidly urbanizing delta cities.

Based on history observations, the intensity of storm-induced rainfall events have increased in recent years (Kossin, 2018; Wang et al., 2019; Chen, 2022). Typhoon rainfalls coinciding with storm surges at coastal areas known as coastal compound flooding significantly exacerbates flooding risks (Wahl et al., 2015; Lin et al., 2010; Du et al., 2020). For example, Hurricane Harvey struck Houston, Texas, in 2017, making landfall three times (Wang et al., 2018). The prolonged cyclone resulted in an accumulated rainfall of 1,318 mm, coupled with multiple high tides that hindered the drainage of inland floodwaters. This severe flooding killed at least 73 people, destroyed 9,000 houses, and resulted in economic losses of $90~160 billion (Wang et al., 2018). Moreover, the combination of basin flooding in river deltas can cause even more significant losses. For example, during the 1997 Typhoon Winnie, heavy rainfall and storm surges combined with major floods from the Yangtze River basin caused the largest compound flooding event in Shanghai since 1949 (Wang et al., 2019). Here, we studied Shanghai, a large delta city built on low-lying estuary, experiencing flooding primarily due to heavy rainfall and levee overtopping from tidal penetration. The global studies by Hallegatte et al. (2013) and Balica et al. (2012) identify the city of Shanghai as one of the world most vulnerable coastal cities to increased flood risk due to climate change and urban development.

In this research, we developed multi-adaptive measures considering local drainage, infrastructure setting, and compound flood characteristics of Shanghai, in light of the rapid urbanizing projection of the delta city. Lingang district (LGZ), designated as an International Pilot Free Trade Zone in Shanghai, is projected to experience rapid urban development in the future (Yin et al., 2019). We investigated both current and future projected socio-economic scenarios based on a land-use change CLUMondo model. Traditional large-scale coastal flooding models often overlook river overtopping process, resulting in inaccurate calculations of fluvial flooding. To address this, we employed a high-resolution ocean-land coupled numerical model that includes all river networks in LGZ. Significant scenarios like the recent Zhengzhou "7·20" rainstorm was assumed to compound with local coastal storms. Notably, our study integrated three flood adaptation measures—heightening seawall and dike (HSD), increasing green area (IGA), and lowering green space (LGS)—into the numerical model to evaluate their flood mitigation effects. The latter two measures are considered low-impact development (LID) strategies. We assessed current and future flooding losses under rapid urbanization by predicting land-use changes and tested the effectiveness of these flood adaptation solutions for future urban planning. Our findings are directly applicable to inform LGZ urban planning in Shanghai and provide valuable insights for constructing flood-resilient cities in estuarine delta regions worldwide.

2. Study area

Shanghai, the largest city in China in terms of economy and population, is located at the mouth of the Yangtze River. This delta city, bordered by the sea on three sides and Taihu Lake on the fourth (Fig. 1), faces one of the highest coastal flood risks among global mega-delta cities (Du et al., 2020; Hu et al., 2019; Wang et al., 2019). The Lingang district (LGZ), designated as an international free trade zone, is rapidly developing and is crucial to Shanghai's socio-economic growth (Yin et al., 2019). Situated in southeastern Shanghai and bounded by the Dazhi and Jinhui Rivers, LGZ covers approximately 819 km^2 and is highly susceptible to compound flooding. The terrain is predominantly low and flat, with an average elevation of only 2~4 m. The total length of all rivers within the LGZ is about 3,150 km, resulting in a river density of approximately 72.4 km/km^2. All rivers in LGZ are protected by sluice gates at their sea entrances (Fig. 1). Historically, this region has been frequently impacted by tropical typhoons, particularly during the summer flood season when storm surge coincides with basin flood, leading to potential compound flooding (Yin et al., 2019). The flood defense system in LGZ has been repeatedly reinforced over the past decades, especially after Typhoon Winnie in 1998 (Yin et al., 2019). However, the current flood defense standards have not fully kept pace with rapid urban development, necessitating enhanced flood defense and water management for effective compound flood defense.

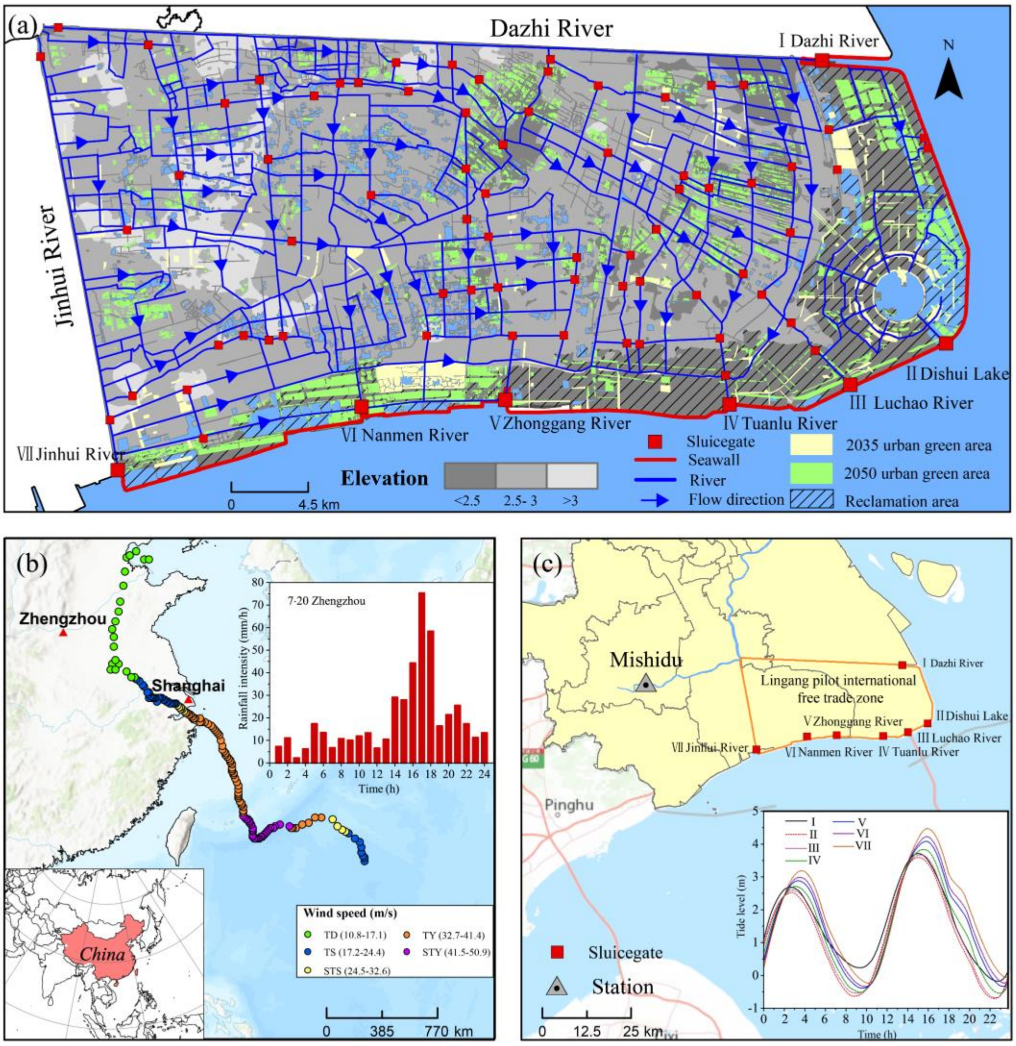

Fig. 1. Study area of Lingang Pilot Free Trade Zone in Shanghai: (a) Geographic map displaying the network of rivers and canals, and key infrastructure of inland sluice gates (small red squares) and tidal sluice gates (big red squares) within the region, (b) Path of Typhoon In-fa in 2021, including rainfall intensity data for Zhengzhou on 20th, July, (c) Recorded tidal levels at tidal sluice gates (I-VII) at the entrance of Dazhi River, Luchao River, Tuanlu River, Zhonggang River, Nanmen River, and Jinhui River during the landfall of Typhoon In-fa in Shanghai on 26th, July.

3. Data and Methods

3.1 Data sources

Reliable flood modeling and evaluation of adaptation measures depends on accurate geometric and hydraulic data. We produced a high precision 20m x 20m digital terrain model (DTM) with the vertical error declared to be less than 0.01 m. The DTM was constructed based on LiDAR aerial photogrammetry and field measurement, depicting building base elevations, by combining RTK measurements with data of topographic map obtained from the Shanghai Institute of Surveying and Mapping (https://www.webmap.cn/). Seawall heights were determined through field measurements conducted in 2019. Information on the urban river network, riverbank elevations, and river profiles was obtained from the Shanghai Municipal Water Affairs Bureau and the Shanghai Municipal Flood

Control Center (https://swj.sh.gov.cn/). Data on the distribution and structure of sluice gates were collected through field measurements in 2019. Tide data during Typhoon In-fa in 2021 was provided by the Shanghai Municipal Water Affairs Bureau (Fig. 1). Hourly precipitation data for the Zhengzhou "7·20" rainstorm event from July 20, 2021, 9:00 AM to July 21, 2021, 8:00 AM, was obtained from the Meteorological Center of the China Meteorological Administration (Fig. 1). Historical land use data for 2013 and 2020, used in the urban-development model, were acquired from the Third National Land Census (https://www.gov.cn/). Additional factors critical for urban-development modeling, such as slope, aspect, railway distribution, and socio-economic data including GDP and population, were sourced from the Geospatial Data Cloud (https://www.gscloud.cn/) and the Seventh Population Census (https://www.stats.gov.cn/).

3.2 Model configurations

3.2.1 Land-use change urban-development model

The CLUMondo model, recognized for accurate predicting of Land Use and Land Cover (LULC) spatial evolution, was employed to forecast future urban development in Shanghai (Domingo et al., 2021; Yang et al., 2022). This model offers detailed spatial outputs and supports scenario analysis by integrating socio-economic and geography drivers, allowing adaption to different economic, environmental, and social conditions (Stehfest et al., 2019). Its adaptability and customizability make it suitable for various land-use dynamics studies (Van and Verburg, 2013; Eitelberg et al., 2015; Domingo et al., 2021; Yang et al., 2022). Integrating local knowledge, fieldwork, and insights from similar studies, we categorize LULC into six types: residential, industrial, agricultural, roads, commercial, and water in this research (Jiang et al., 2021). The urban expansion modeling was driven by LULC demand, which is determined using algorithms and driving factors to meet GDP growth projections (Liao et al., 2022; Stehfest et al., 2019). Given geographical and socio-economic factors are primary drivers of LULC change, this study identifies seven driving factors—DEM, slope, aspect, GDP, population, distance from railway, and distance from river—based on the 2020 land use distribution to project changes for 2035 and 2050.

Essentially, the CLUMondo model operates with a non-spatial demand module and a spatial allocation module (Wolff et al., 2018; Yang et al., 2022). Key parameters include land-use demand, conversion resistance, and a conversion matrix. Initially, CLUMondo facilitates spatial allocation through empirical spatial analysis and dynamic land-use modeling. The primary driver of land-use change is the demand for regional socio-economic factors and services, such as crops, livelihoods, and construction (Hasan et al., 2020). Additionally, external resource demand generates competition among different land-use types (Smith et al., 2010). In this study, the area of built-up land (e.g., residential, industrial, roads, and commercial) is used to represent regional land-use demand. Then, the conversion resistance, referring to the reversibility of LULC changes, is configured by transfer-out costs and the reversibility of land-use types, ranging from 0 (easy) to 1 (difficult). Finally, the conversion matrix specifies whether conversions between different land classes are permitted, with values of 0 (conversion not allowed) and 1 (conversion allowed). This structured approach enables accurate forecasting of urban development patterns and supports effective planning for future land use changes in Shanghai.

3.2.2 Hydrodynamic compound flood model

The hydrodynamic compound flood model used in this study is based on the DHI MIKE modeling suite, which includes modules for simulating ocean, coastal, and urban flood processes (Du et al., 2020; Wang et al., 2019). The performance of MIKE modeling suite is widely recognized for its robustness in simulating complex hydraulic and hydrological processes in coastal, fluvial, and pluvial conditions (DHI MIKE, 2011; Jiang et al., 2021; Wang et al., 2019). Firstly, the MIKE11 fluvial model is developed using a one-dimensional grid to ensure efficient large-scale basin river computation. High-resolution LGZ river network, covering approximately 992 km, is discretized into 758 sections with profiles derived from field surveys. River profile positions and riverbank heights are interpolated from upstream and downstream cross-sections and defined at key nodes along the river network. Boundary conditions such as sluice gates and open boundaries are applied to the lower (ocean) and upper (basin) reaches of the river, respectively. Secondly, a two-dimensional finite element coastal and pluvial model, MIKE21, is implemented with a grid comprising 4 million cells to numerically solve the complete 2D Saint-Venant equations (DHI MIKE,2011; DHI, 2016). The rectangular grid is optimal for urban landscape flood simulation, with the Manning coefficient assigned reflecting different land-use types according to CLUMondo model in 2020, 2035, and 2050 (Du et al., 2020; Wang et al., 2019). Processes such as rainfall-runoff and evaporation-infiltration are also integrated into the MIKE21 model.

To implement compound coastal, fluvial, and pluvial flood simulations, a MIKE FLOOD module has been developed, integrating MIKE11 and MIKE21 into a comprehensive flood simulation system, allowing for the nesting of small-scale urban flood model within the large-scale coastal and basin-river flood models (Du et al., 2020; Wang et al., 2019). The module facilitates seamless interaction between MIKE11 and MIKE21, enabling the transfer of driving forces through standardized data input and output formats (Wang et al., 2019). The connection between MIKE11 fluvial and MIKE21 coastal flood models is established through lateral coupling across computational grids on both sides of the riverbanks through a two-way coupling method. The CELLTOCELL (weir flow formula) approach links dike heights in the MIKE11 river channel with the MIKE21 floodplain grid, effectively managing dynamic boundary conditions with a dry-wet grid method (DHI, 2016; Wang et al., 2019). This approach, determining water flow direction based on the difference between water level and dike height, is particularly effective for simulating scenarios involving river overtopping (DHI, 2016; Wang et al., 2019).

3.3 Model calibration and validation

3.3.1 Urban-development model validation

Urban-development CLUMondo model, starting with the 2013 land-use data, was used to predict future urban expansion until 2050 and validation by comparing to actual land-use distribution in 2020. The 2013 LULC data, along with dominant driving factors as discussed above, were input into the CLUMondo model. Then, the model ran iteratively using customized conversion resistance matrix and LULC demand parameters to predict the 2020 distribution. The process continued until the model achieved an AUC (Area Under the Curve) value reaching between 0.6 and 0.82, indicating a moderate to good performance (Yang et al., 2022). The selection of LULC demand algorithms was based on historical trends (2013-2020), extrapolated to forecast future demand according to the growth rate of built-up land, including industrial, residential, roads, and commercial areas (Liao et al., 2022; Yang et al., 2022). The conversion matrix and resistance values were initially based on historical land-use calibration and were then adjusted for current and future conditions based on updated LULC demand.

To validate the model, the predicted 2020 land use was compared with the actual 2020 land-use map using Map Comparison Kit 3.0 (Visser and de Nijs, 2006). Initially, conversion resistance was set to 0, prohibiting conversion for residential, industrial, roads, and commercial areas, while other LULC types were set to 1, allowing conversion. After calibration, the conversion resistance values were modified to 0.76 for residential, 0.6 for industrial, 0.4 for agricultural, 0.92 for roads, 0.93 for commercial, 0.79 for green space, and 0.7 for water. The comparison yielded a Kappa coefficient of 0.85 and a FOM (Figure of Merit) index of 0.08, indicating high model accuracy. Such careful calibration and validation ensured that the CLUMondo model could accurately predict land-use changes, supporting effective flood propagation model and damage investigation in the rapidly developing delta city of Shanghai.

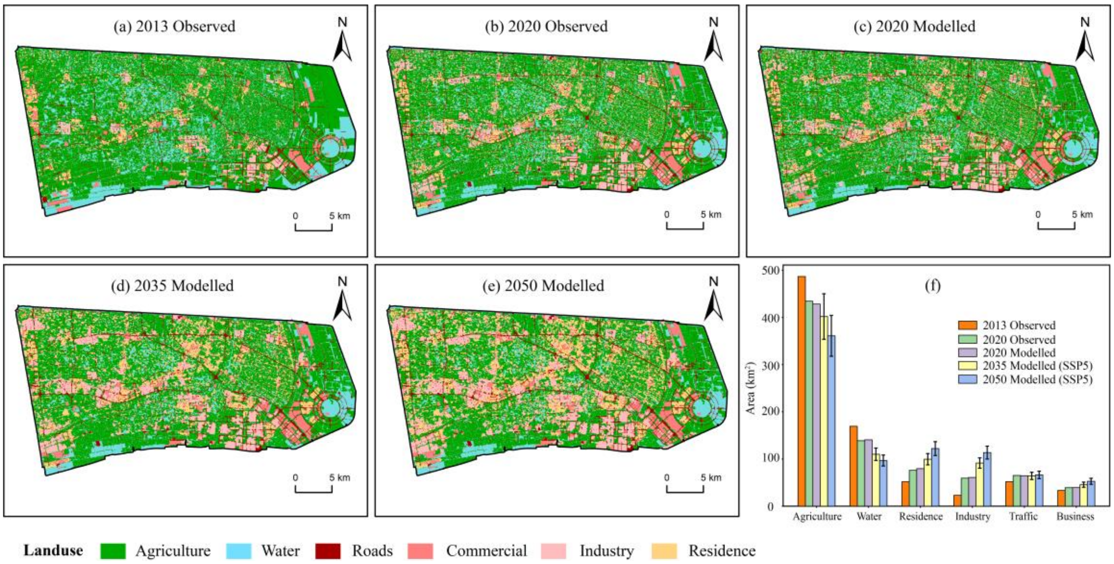

Fig. 2. Land use distribution map: (a-b) Observed land use distribution for 2013 and 2020, (c-e) Modeled land use distribution for 2020, 2035 (SSP5 scenario), and 2050 (SSP5 scenario). (f) Land use area statistics for each year, with the upper and lower boundaries representing the SSP1 and explosive growth scenarios, respectively.

3.3.2 Hydrodynamic model validation

The hydrodynamic flood propagation models were calibrated and validated using measured river water levels and flood areas during Typhoon In-fa in 2021. The typhoon, analyzed as a case study, caused storm surges, heavy rainfall, and upstream fluvial flooding, raising water levels in the middle reaches of the Huangpu River. Hourly water levels measured at the Mishidu Hydrological Station (Fig. 1c) were used to calibrate and validate the one-dimensional MIKE11 model (fluvial flood model). Result show that the model accurately captured key fluctuations in water levels, achieving a RMSE (root mean square error) below 0.01, indicating minimal discrepancies between simulated and observed water levels (supplementary Fig. S1). To validate the compound coastal flooding model, we used reported urban flooding area during Typhoon In-fa. Flood areas reported by 110 emergency alarms, news reports, and newspapers were compared with the model's results (supplementary Fig. S2). The simulated flooding areas closely matched the reported waterlogging regions located 1 to 6 in LGZ during the typhoon, confirming the reliable compound flooding simulation.

3.4 Scenario simulation

3.4.1 Single and compound flood scenarios

Typhoon In-fa in 2021 resulted in 283.8 mm of cumulative precipitation in Shanghai from July 23 to 27. Additionally, Typhoon In-fa’s storm surge coincided with local astronomical high tide, raising the compound storm water level to 5.49 m at the Huangpu Park station, equivalent to 200-year return level periods (SMOB, 2021). The residual circulation of Typhoon In-fa and Cempaka indirectly affected the heavy rainfall in Chinese Zhengzhou, Henan Province through water vapor transport, causing a historically rare heavy rainstorm in Zhengzhou, with the maximum hourly rainfall intensity reaching 201.9 mm, equivalent to 500-year return level periods (ZBNRP, 2023), resulting in 398 deaths, affecting approximately 15 million people, and direct economic losses of $17.4 billion RMB, known as the Zhengzhou “7·20” rainstorm disaster (Ministry of Emergency Management, PRC).

Based on Zhengzhou “7·20” rainstorm event, two flood scenarios were designed to test the effectiveness of flood adaptation measures in Shanghai (see Table in Fig. 3): (a) **Single Heavy Rainfall Scenario (SHR Scenario)**: This scenario uses rainfall data from the Zhengzhou "7·20" rainstorm event as the primary flood-driving factor (see Fig. 1b). The evaluation considers the impact of heavy rainfall while maintaining the current dike heights and keeping the river channel sluice gate opened. (b) **Compound Storm Surge and Rainstorm Scenario (Compound Scenario)**: This scenario combines the storm surge from Typhoon In-fa (see Fig. 1c) with the rainfall data from the Zhengzhou "7·20" rainstorm event. The assessment considers the impact with the current dike heights and the river channel sluice gate open. This configuration allows the storm surge to penetrate tidal rivers, including the Dazhi River, Dishui Lake, Luchao River, Tuanlu River, Zhonggang River, Nanmen River, and Jinhui River (see Fig. 1a). Additionally, the upstream boundaries of the Dazhi and Jinhui Rivers, which are connected to the Huangpu River, are set as open discharge boundaries using measured time-series river flow during the event.

3.4.2 Flood simulation with adaptation

The designed flood adaptation measures include both soft and hard engineering strategies, specifically: heightening seawalls and dikes (HSD), increasing green area (IGA), and lowering green space (LGS) (refer to Fig. 3 for the conceptual model diagram). HSD represents a traditional hard engineering method, while IGA and LGS are classified as Low Impact Development (LID) measures under the sponge city concept (Hu et al., 2019). The specific configurations are detailed below:

(a) **HSD:** This involves increasing the current dike height by 0.2 m ~ 0.5 m to evaluate the impact on mitigating SHR and compound floods.

(b) **IGA:** Based on the 2035 LGZ urban planning map (IGA-I) and 2050 CLUMondo urban-development modeling (IGA-II), public green spaces and farmland in severely inundated areas were converted to green spaces with enhanced infiltration capacity. After implementing IGA, the soil infiltration rate for the selected green spaces was set to 10 mm/h, a significant improvement compared to the low permeability of urban areas affected by human activities.

(c) **LGS:** In addition to the functions of IGA, the green areas were lowered by 0.5 m ~ 1 m as a flood storage and retaining area to test the sensitivity of reduced land elevation on flood mitigation.

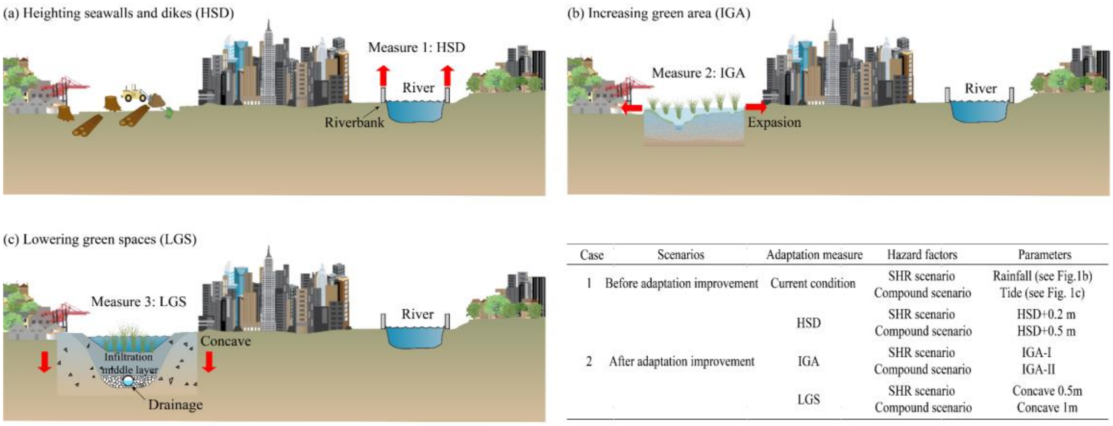

Case	Scenarios	Adaptation measure	Hazard factors	Parameters
1	Before adaptation improvement	Current condition	SHR scenario Compound scenario	Rainfall (see Fig.1b) Tide (see Fig. 1c)
2	After adaptation improvement	HSD	SHR scenario Compound scenario	HSD+0.2 m HSD+0.5 m
		IGA	SHR scenario Compound scenario	IGA-I IGA-II
		LGS	SHR scenario Compound scenario	Concave 0.5m Concave 1m

Fig. 3. Conceptual model of the tested adaptation measures. HSD represents the strategy of heightening seawalls and dikes to prevent coastal and river overtopping. IGA involves increasing green area to enhance soil infiltration, as illustrated by the projected urban green area for 2035 and 2050 shown in Fig. 1c. LGS refers to lowering green space by creating concave landscapes to retain the flooding water.

3.4.3 Future socio-economic scenario

In this section, we use the Shared Socioeconomic Pathways (SSPs) framework and GDP growth rates to estimate future asset values in Shanghai (Jiang et al., 2021). We calibrated key socioeconomic parameters—such as labor input, total productivity factor, and capital stock—using the Cobb-Douglas economic forecasting model, drawing on data from Shanghai's population censuses and economic statistical yearbooks to project potential economic trends and their implications for asset valuations. Based on historical GDP data (1990-2020) for LGZ (SMBS, 2023), we projected future asset values under three socio-economic scenarios (Fig. 4): sustainable development (SSP1), conventional development (SSP5), and explosive development for 2035 and extending to 2050 with different growing rate (Jiang et al., 2018a). We then estimated the spatial distribution of asset values in LGZ for 2035 and 2050 under these scenarios using the CLUMondo model (Fig. 2). This approach allows to understand how different development pathways could impact the distribution and value of social assets in Shanghai over the coming decades.

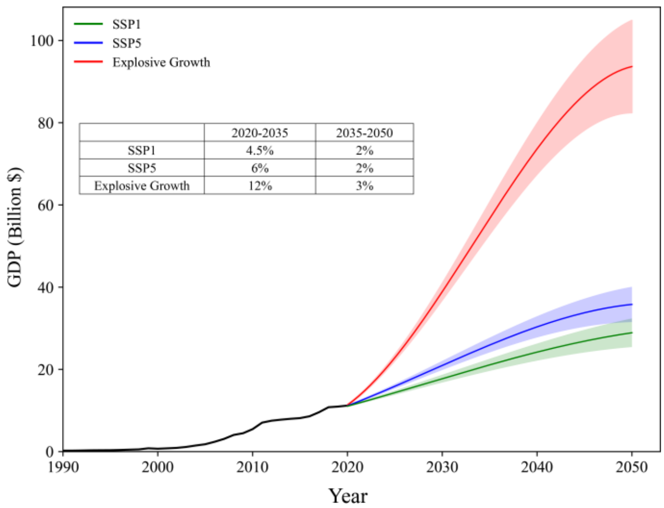

Fig. 4. Scenario-based GDP forecast in Shanghai Lingang Pilot Free Trade Zone for the period 2020-2050. The figure illustrates GDP projections under three different scenarios: SSP1, SSP5, and explosive growth. The solid lines represent the median GDP values, while the shaded areas indicate the 95% confidence interval. The accompanying

table shows the average annual growth rates for two sub-periods, 2020-2035 and 2035-2050, highlighting the differences between each scenario.

3.5 Asset exposure and loss calculations

Asset exposure to flooding is assessed by identifying grid cells with a flood depth of 0.3 m (about 1 foot) or more, based on practical considerations of damage to structures and vehicles as well as human safety, following Flood Risk Mapping Standards of the People's Republic of China (Guidelines for Flood Risk Mapping, 2017). This evaluation includes assets in residential, industrial, agricultural, roads, and commercial sectors, while excluding green spaces and water bodies. Using ArcGIS software, we performed raster calculations to determine both current and future asset exposure under present and adaptation conditions. For asset loss analysis, we evaluated damage based on vulnerability curves specific to various land-use types, as outlined by Yin et al. (2012). The simulated flood inundation extent was overlaid with the spatial asset distribution map. By multiplying the inundation depth with the asset distribution, we calculated direct economic losses, employing the vulnerability curves for each land-use category (supplementary Fig. S3).

$$E = G \cap H \tag{1}$$

where, E is the total exposed asset, G is the asset spatial distribution, and H is the flooding area.

The asset losses for each land-use type are assessed by integrating the exposed assets and vulnerability curves considering flooding depth.

$$d(x) = \int_0^x v_{(x)}\, E dx \tag{2}$$

where, $v_{(x)}$ is the vulnerability curve of various land use types, and x is inundation depth. This approach ensures a comprehensive assessment of potential flood impacts on different sectors within Shanghai.

4. Results

4.1 Compound flooding in Shanghai

Modeling results reveal that an extreme rainstorm, similar to the Zhengzhou "7·20" rainstorm event, could lead to severe urban flooding in Shanghai. In such SHR scenario, 219 km² (27%) of LGZ would be submerged, with water depths exceeding 0.3 m (see supplementary Table S1). Flooding would be more severe in the eastern and southern coastal areas compared to the western and northern inland regions, primarily due to topographical constraints. Severely inundated areas, mainly in coastal regions and inland areas, would experience water depths of 0.3 to 0.5 m, covering 103.7 km². Areas with water depths exceeding 0.5 m are relatively limited, representing 6% of the flooded region. These areas are primarily located in towns with dense river networks and low elevations, where fluvial floods accumulate and cause significant river overtopping. Most areas experiencing severe flooding depths exceeding 1 m consist of low-lying farmland. In contrast, buildings and towns typically face shallower flooding, generally not exceeding 0.5 m.

The compound flood modeling reveals a significant increase in inundation area deeper than 0.3 m, reaching 349 km², which is 16% greater than the area affected under the SHR scenario (see supplementary Table S1). Severe flooding, with depths exceeding 0.5 m, expanded by an additional 94.5 km² in the coastal zone. Moreover, the joint zone between the coastal and inner regions, with flood depths exceeding 0.5 m, expanded to cover 130 km². Flood source tracking analysis indicates that seawall overtopping is minimal, underscoring the critical role of coastal embankments in flood mitigation. Although coastal areas are protected by seawalls, there are seven river sluice gates evenly distributed along the LGZ coast, which serve as the main channels for ocean tide intrusion. The storm surge from Typhoon In-fa transformed into high tides, leading to a considerable seawater influx into tidal rivers. This influx, combined with basin floodwater from the Huangpu River, resulted in the overtopping of riverbanks and rapid expansion of flooded areas. Therefore, coastal flooding notably exacerbates fluvial and pluvial flooding through tidal penetration and backwater effects via tidal rivers. Flood propagation analysis shows that the polder effect amplified the compound flooding, where waterlogging is obstructed by the seawall around the Yangtze River Delta.

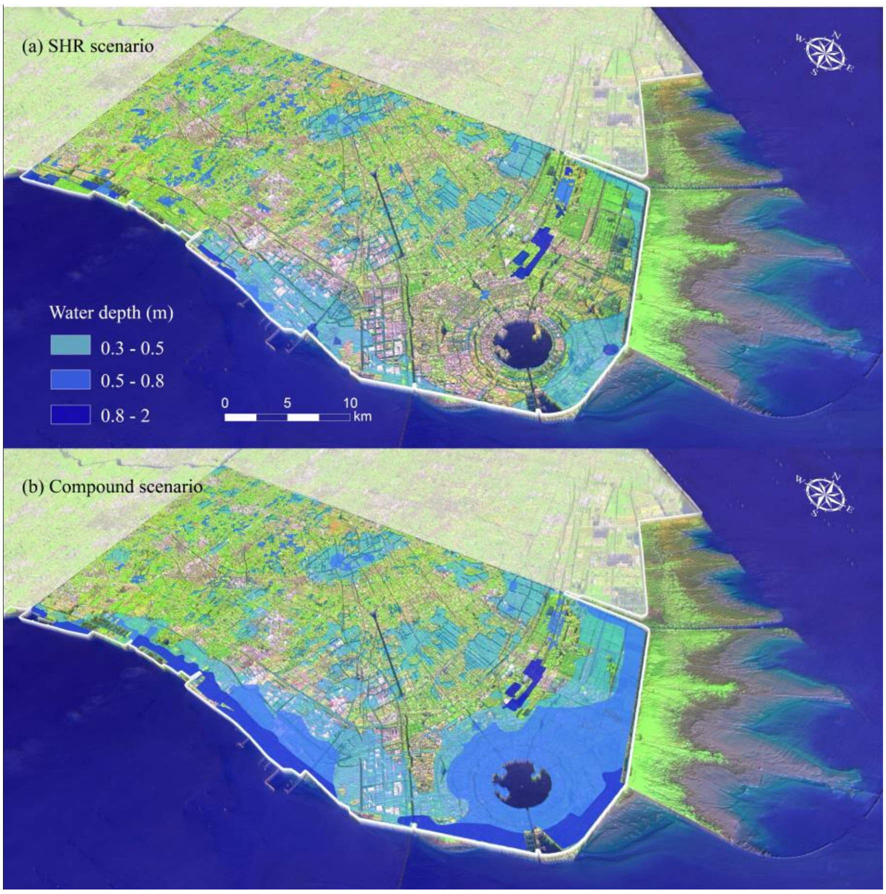

Fig. 5. Three-dimensional view of flooding distribution in the Shanghai Lingang Pilot Free Trade Zone under (a) Single Heavy Rainfall Scenario (SHR scenario) and (b) compound scenario.

4.2 Flood adaptation measures

Three adaptation solutions were assessed for their efficacy in mitigating SHR and compound flooding in LGZ. The first solution, HSD effectively reduces fluvial flooding by preventing river overtopping. A 0.5 m increase in HSD height reduces the flooding area in LGZ by 24% compared to a do-nothing scenario, equivalent to 83 km^2. This reduction is particularly notable in coastal and western inland areas where flooding is most significant. The second solution, LID strategies, includes IGA and LGS. IGA-I enhances rainwater infiltration and aquifer retention, reducing the flooding area by 15% and IGA-II further reduced flooding area by 20%. This strategy significantly decreases flooding around Dishui Lake but has less impact on other coastal areas. Conversely, LGS is highly effective in reducing waterlogging. Lowering LGS by 0.5 m reduces flooding near Dishui Lake to less than 0.3 m. Further lowering LGS to 1 m decreases the flooding area by 21% (see supplementary Table S1). Thus, LGS 1 m proves more effective in waterlogging removal compared to IGA-II and HSD 0.5 m (see Fig. 6).

Although the three adaptation solutions exhibit similar flood mitigation functions in coastal areas, their effectiveness varies for the inland areas (see Fig. 6). Modeling results show that the most effective measures for flood risk reduction are LGS 1 m, HSD 0.5 m, and IGA-II, reducing compound scenario flooding by 51%, 24%, and 20%, respectively. Thus, LGS emerges as the most effective solution for reducing flooded areas. While HSD is less effective in reducing pluvial waterlogging may also require additional pumping stations for optimal regional water removal, it effectively prevents river overtopping from tidal penetration-induced fluvial flooding. Conversely, IGA and LGS primarily mitigate waterlogging from rainfall-runoff. Although these low-impact development measures cannot prevent flooding from entering the city, they retain water in aquifers and concave low-lying spaces, reducing urban waterlogging by redirecting flooding via roads and squares to surrounding green areas. Considering the multifunctional flood mitigation functions of LID measures on coastal, fluvial, and pluvial flooding, LGS and IGA shows significant potential for integration into future urban landscape planning focused on low-impact development.

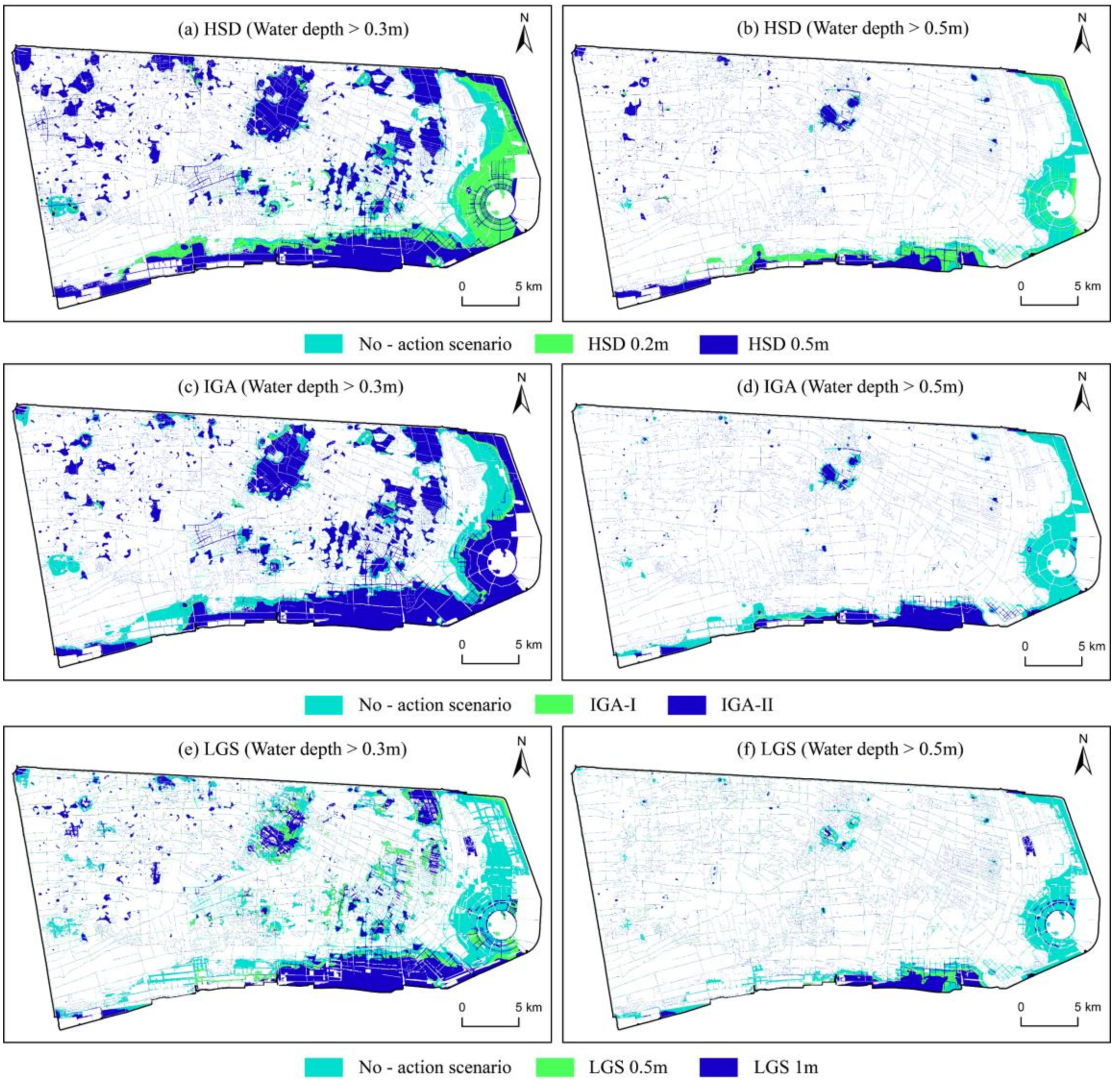

Fig. 6. Comparison of flooding depth distribution in Shanghai Lingang Pilot Free Trade Zone for the adaptation measures of (a, b) heightening seawall and dike (HSD) by 0.2~0.5 m, (c, d) increasing green area (IGA), and (e, f) lowering green spaces (LGS) by 0.5~1 m illustrated in Fig. 3. The maps illustrate water depth distributions for flood depths greater than 0.3 m and 0.5 m under no-action scenarios and the corresponding adaptation measures,

highlighting their effectiveness in reducing flood risk.

4.3 Asset exposure amplification and adaptation

Numerical model calculation indicates that assets valued at $4 billion are currently exposed to the SHR scenario in the LGZ area. In the compound flooding, this exposure could potentially nearly double, increasing to $7 billion. As urbanization continues under Shared Socioeconomic Pathways (SSP1 to SSP5) scenarios and particularly under the potential explosive growth scenarios, asset exposure is projected to significantly increase in the future (Fig. 7). Specifically, for compound flooding, exposure is expected to rise by 360% by 2035 and further by up to 820 % by 2050, reflecting the intensified risk with ongoing urban expansion. Modeling on asset exposure across different land-uses indicates that, in 2020, the land-use types most exposed to flood risks were industry and agriculture, accounting for 24% and 27% of the total exposure in LGZ. As urbanization progresses, in the future the exposure profile is anticipated to shift, with industry and residence becoming the most exposed, increasing to around 45% and 22% by 2050. Conversely, the proportion of agriculture exposure is expected to decline and become the smallest, accounting for only 5% in 2050, reflecting the ongoing conversion of agricultural land to other uses. Notably, the magnitude of increase in exposure for land-use of industry or residence is 18 or 8 times the decrease in agriculture's exposure, highlighting a disproportionate acceleration amplification in asset exposure across different land-uses.

Our analysis of mitigation measures on asset exposure across different land-uses shows that adaptation measure of LGS outperforms HSD and IGA in flood mitigation. However, the effectiveness is highly dependent on specific parameter configurations. Measures with higher HSD, larger IGA, and lower LGS provide better flood mitigation but are constrained by construction costs, space availability, and urban landscape design considerations (Fig. 8). For example, in 2020, implementing HSD measures at different heights (0.2 m~0.5 m) could reduce compound flooding exposure by 7%~39%. IGA of different scale ($18.1km^2$ ~ $61km^2$) could reduce exposure by 19%~28%, while LGS measures at 0.5m~1m could reduce exposure by 50%~67%, making LGS at 1 m the most effective in reducing current asset exposure (Table 1). Looking forward, under SSP1, SSP5, and explosive growth scenarios, the effectiveness of these adaptation measures intensifies. For example, compared to 2020, HSD at 0.5 m could reduce exposed assets increased by 4.5 times by 2035 and by 8.8 times by 2050 (Table 1). IGA-II and LGS 1 m measures also show significant potential to reduce asset exposure (Table 1), particularly for industry assets (Fig. 7). Specifically, LGS at 1 m could reduce industry asset exposure by $1 billion in 2020 and by $6 billion, $7 billion, and $19 billion under different scenarios by 2050. To ensure the safety of future industrial development and support the harmonious growth of a green economy, we recommend integrating LGS measures with urban park planning as part of a long-term sustainable development strategy.

Table 1. Current and future asset exposure (billion $) across various socio-economic development scenarios and adaptation measures (HSD, IGA, and LGS) with parentheses show 95% confidence interval.

Exposure asset	2020	2035			2050		
(billion $)		SSP1	SSP5	Explosive growth	SSP1	SSP5	Explosive growth
SHR scenario	4	6 (4~9)	8 (5~11)	16 (11~23)	11 (7~16)	13 (8~19)	33 (20~48)
Compound scenario	7	13 (8~18)	16 (10~22)	33 (22~46)	22 (13~31)	27 (16~38)	66 (41~97)
HSD 0.2m	7	12 (8~16)	15 (9~20)	31 (20~43)	20 (12~29)	25 (15~35)	61 (38~90)
HSD 0.5m	4	8 (5~11)	10 (6~14)	21 (13~28)	14 (8~20)	17 (10~24)	42 (26~61)
IGA-I	6	10 (7~14)	13 (8~17)	27 (17~37)	17 (11~25)	21 (13~30)	53 (33~78)

IGA-II	5	9 (6~13)	11 (7~16)	24 (16~34)	16 (10~23)	19 (12~28)	48 (30~71)
LGS 0.5m	4	6 (4~9)	8 (5~11)	17 (11~23)	11 (7~16)	14 (8~20)	34 (21~50)
LGS 1m	2	4 (3~5)	5 (3~7)	10 (7~14)	7 (4~10)	8 (5~12)	19 (12~27)

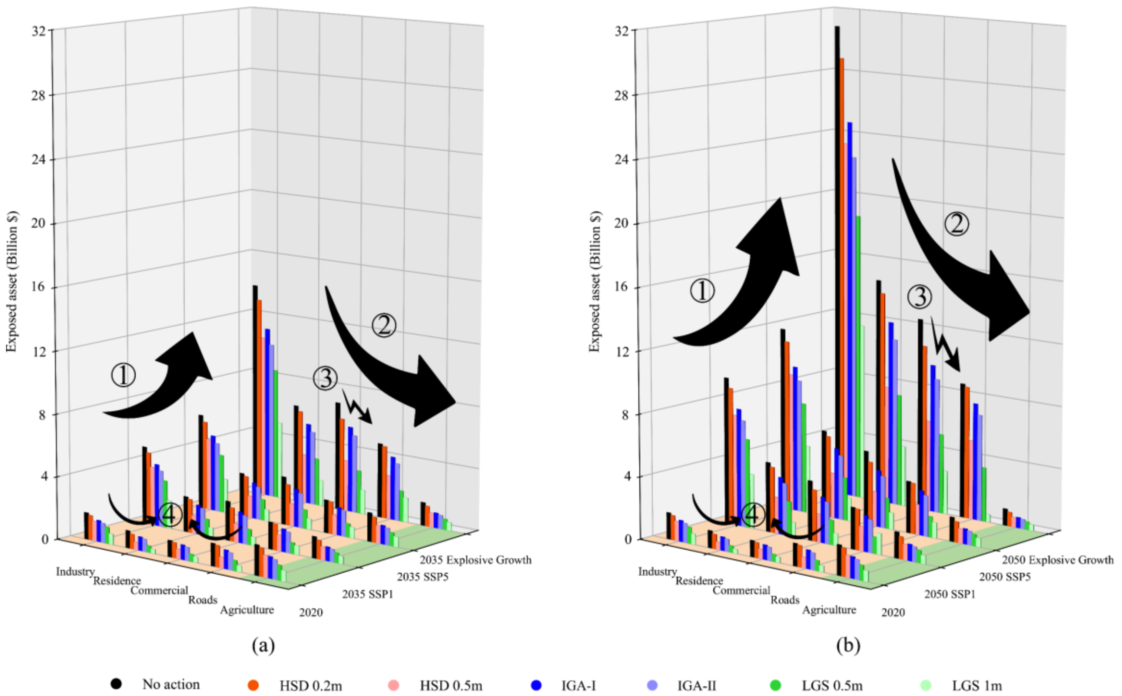

Fig. 7. Comparison of current and future asset exposures in the Shanghai Lingang Pilot Free Trade Zone under various adaptation measures versus a no-action scenario. The charts illustrate the estimated exposed asset (in billions $) across different sectors (industry, commercial, roads, residence, agriculture) for two future timeframes (2035 and 2050) under scenarios such as HSD 0.2m, HSD 0.5m, IGA-I, IGA-II, LGS 0.5m, LGS 1m, and the no-action scenario. The left chart shows projections for 2035, while the right chart depicts projections for 2050, both considering SSP1, SSP5, and explosive growth conditions. Arrows indicate ① trends of increasing exposure with urbanization acceleration, ② the impact across different sectors, ③ differences in effectiveness between adaptation measures, and ④ exposure across different sectors in 2020.

4.4 Asset losses amplification and adaptation

Unlike asset exposure, which only considers the presence of assets in flood-prone areas, asset loss evaluates the damage based on specific water depths. According to the inundation loss curve, losses tend to increase linearly with greater water depths. Therefore, assessing asset loss requires focusing on the distribution and types of assets in areas experiencing significant inundation. Under compound flood scenarios, regions with water depths exceeding 0.5 m are primarily found along the northern coast of Hangzhou Bay (Fig. 6). This region, the previous mudflats, was reclaimed and initially converted into farmlands (Fig. 1a). With the establishment of the Pilot Free Trade Zone in 2019, the new city's development has transformed the area into high-tech development zones with industrial parks, commercial, and residential areas (Fig. 2). These new districts, unlike older urban areas, are characterized by high technology and significant asset value, making them especially vulnerable to flooding, particularly deep-water inundation. For instance, the Ocean New City—Lingang Dishui Lake area is among the five major new cities prioritized for development in Shanghai; The LGZ on the northern coast of Hangzhou Bay establishes the Tesla Gigafactory Shanghai completed in 2019. This region also includes critical infrastructure such as sewage treatment plants, petrochemical facilities, and key hazardous chemical enterprises.

Future asset losses in Shanghai are projected to increase significantly, particularly under scenarios of explosive economic growth (see Table 2, Fig. 8). By 2035, losses could rise by 42%, 65%, and 214% under Shared Socioeconomic Pathways (SSP1 to SSP5) and especially for explosive growth scenario. By 2050, these figures could further escalate by 74% ~ 292%, representing 0.3~0.4% of GDP, indicating a substantial rise in risk associated with continued urban expansion. Analysis of different land uses in 2020 reveals that agriculture and industry were the most vulnerable to flood risks, contributing to 43% and 22% of the total potential losses in LGZ (Fig. 8). As urbanization continues, the most affected land-uses are predicted to shift, with agricultural asset losses decrease significantly from $233 million in 2020 to $179 million in 2035 and $128 in 2050. By 2035, industry and residential areas are expected to become the most vulnerable, increasing their share to 34% and 28%, and by 2050, these figures could reach 38% and 32%, respectively. In various scenarios, road asset losses remain minimal. Based on the adaptation measures of HSD, IGA, and LGS for proactive asset explore protection analysis as discussed above, it is evident that asset loss mitigation shows a similar effect across these measures. Therefore, in addition to conventional hard engineering measures like HSD, effective LID measures such as IGA and LGS can be implemented around industrial, agricultural, and commercial areas to mitigate asset loss.

Table 1. Current and future asset loss (million $) across various socio-economic development scenarios and adaptation measures (HSD, IGA, and LGS) with parentheses show 95% confidence interval.

Loss asset (million $)	2020	2035			2050		
		SSP1	SSP5	Explosive growth	SSP1	SSP5	Explosive growth
SHR scenario	241	324 (210~450)	374 (243~519)	714 (463~988)	493 (303~715)	599 (368~869)	1393 (861~2035)
Compound scenario	546	777 (505~1077)	899 (584~1248)	1715 (1111~2374)	1171 (720~1689)	1424 (876~2064)	3309 (2045~4834)
HSD 0.2 m	469	653 (424~907)	756 (491~1050)	1444 (936~1999)	988 (608~1439)	1203 (740~1745)	2808 (1735~4102)
HSD 0.5 m	312	415 (269~443)	478 (311~664)	903 (585~1251)	633 (390~918)	738 (454~1070)	1789 (1106~2613)
IGA-I	382	525 (341~728)	622 (404~863)	1209 (783~1376)	815 (501~1182)	997 (613~1446)	2354 (1455~3438)
IGA-II	347	477 (310~662)	565 (367~785)	1099 (712~1251)	741 (456~1075)	906 (557~1314)	2140 (1322~3125)
LGS 0.5 m	260	360 (234~500)	415 (270~576)	781 (506~1082)	556 (342~806)	673 (414~977)	1553 (960~2268)
LGS 1 m	211	249 (162~345)	282 (183~392)	506 (328~702)	371 (228~539)	445 (273~645)	992 (613~1449)

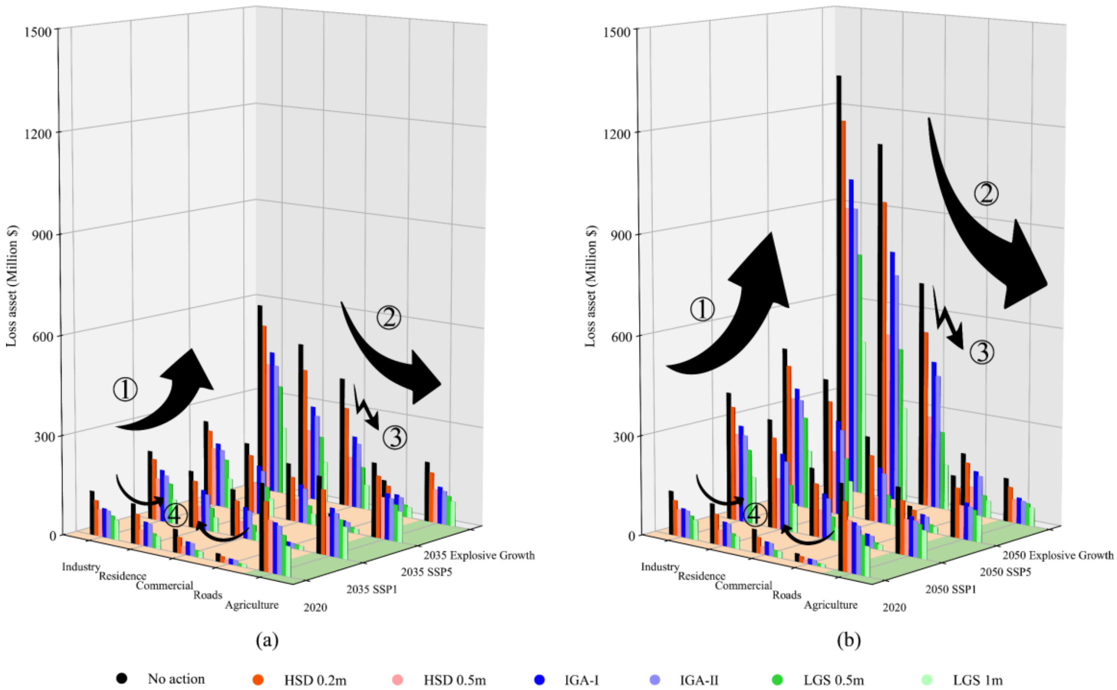

Fig. 8. Comparison of current and future asset loss in the Shanghai Lingang Pilot Free Trade Zone under various adaptation measures versus a no-action scenario. The charts illustrate the estimated loss assets (in million $) across different sectors (industry, commercial, roads, residence, agriculture) for two future timeframes (2035 and 2050) under scenarios such as HSD 0.2m, HSD 0.5m, IGA-I, IGA-II, LGS 0.5m, LGS 1m, and the no-action scenario. The left chart shows projections for 2035, while the right chart depicts projections for 2050, both considering SSP1, SSP5, and explosive growth conditions. Arrows indicate ① trends of increasing loss over urbanization acceleration, ② the impact across different sectors, ③ differences in effectiveness between adaptation measures, and ④ loss across different sectors in 2020.

4.5 Flood risk amplification mechanism

The analysis of flood risk amplification mechanisms reveals that under rapid urbanization in the LGZ, particularly after 2035, both flood exposures and losses increase are expected to accelerate (Fig. 9a, g). The projected economic growth in the LGZ, driven primarily by international free trade potential, will be accompanied by industrial development and a rapid GDP increase (Fig. 2, 4). This growth is leading to a significant expansion in industrial, residential, and commercial areas, which have increased by 48% of the area in LGZ. The conversion of low-valued agricultural land to high-valued industry and residence land-uses is a key factor for the increase in the assets at risk. Specifically, compared to 2020, the assets exposed and lost in industrial and residential areas are projected to be more than triple by 2035 and increase tenfold by 2050. These two land-use types are anticipated to account for over two-thirds of the total flood risk in the LGZ, with industry contributing 36% and residential areas 30%. In contrast, agricultural losses are initially high, reaching 43%, but show a slow increase followed by a rapid decrease to only 4% in 2050 (refer to Fig. 9l). However, the future of the LGZ as an urban economic zone focused primarily on high-valued industry and residential service suggests that the reduction in low-valued agricultural losses will not significantly impact the overall amplification trend in exposure and losses in the LGZ area.

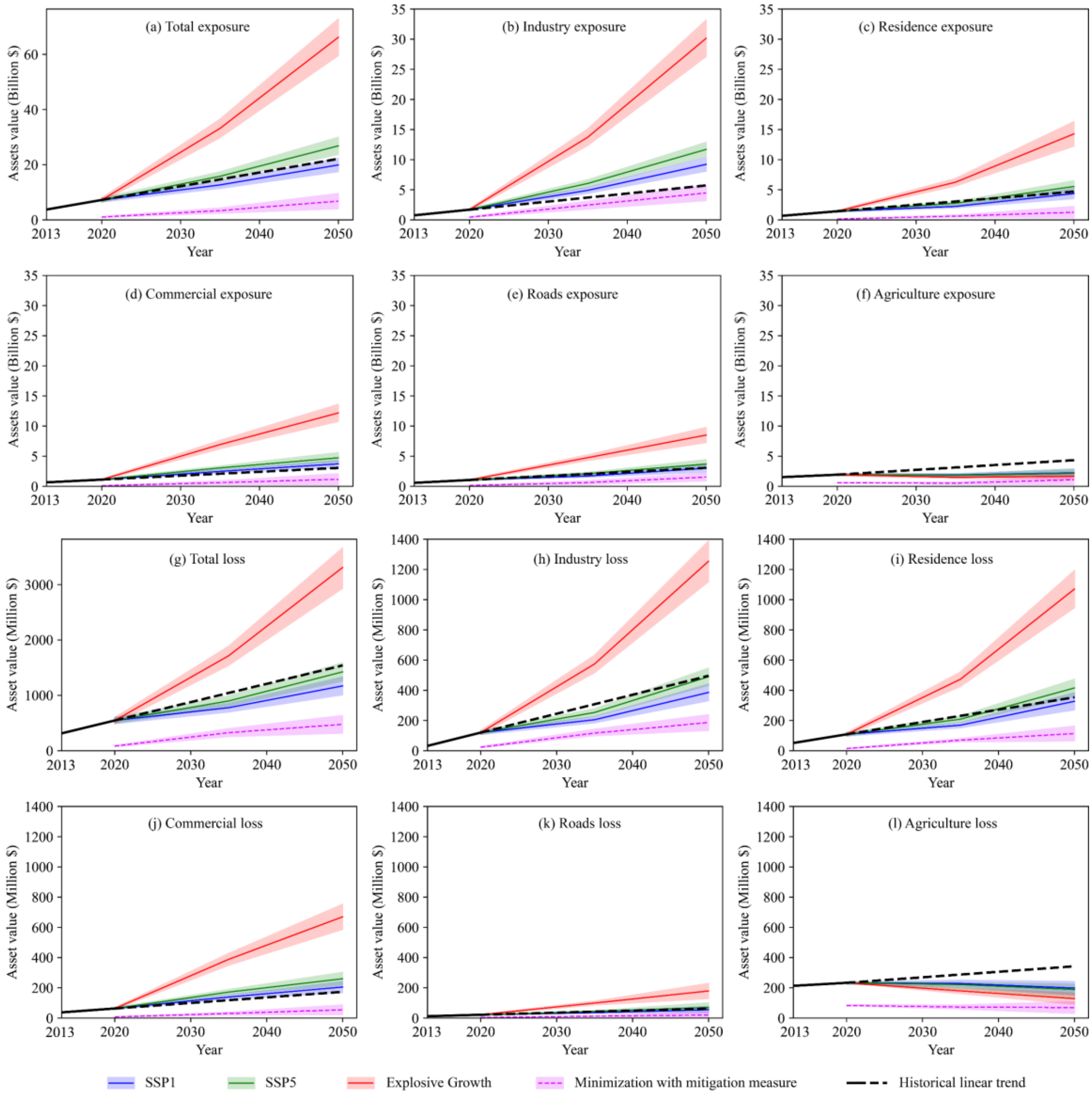

Fig. 9. Historical trends (2013-2020) and projected asset exposures (a-f) and asset losses (g-l) across various sectors (industry, residence, commercial, roads, agriculture) from 2020 to 2050 under different socioeconomic growth scenarios and the mitigation measure. The shaded area represents the 95% confidence interval.

4.6 Urban flood adaptation planning

Adopting integrated approaches to urban planning is essential to address both the immediate and long-term flooding challenges posed by urbanization. The flooding challenges faced by Shanghai highlight the need for robust flood management strategies that combine traditional engineering solutions with green infrastructure. We proved that the implementation of green spaces, permeable surfaces, and LID solutions, such as IGA and LGS, can significantly reduce flood risks. Based on the Land and Space Master Plan for the International Pilot Free Trade Zone of Shanghai (2019-2035), the urban parks and green spaces are mainly located around developed areas (pink area in Fig. 10). Our research shows that increasing these green spaces in the highlighted red zones significantly reduces the pluvial flooding risks. Therefore, we recommend expanding green spaces in these areas to enhance flood mitigation and ecological functions. Additionally, strengthening the endangered riverbanks of the highlighted blue sections is essential to prevent fluvial overtopping (Fig. 10). By a combination of these measures, the flooding to LGZ could be significantly reduced. The benefits of these flood adaptation measures go beyond reducing asset exposure and economic losses; they also improve the ecological environment and support sustainable urban development. By integrating innovative urban flood control planning and prioritizing ecological sustainability, the urban center of Shanghai can be better protected in the context of rapid urbanization.

Fig. 10. Suggested improvement for the Land and Space Master Plan of the International Pilot Free Trade Zone (2019-2035) based on optimizing flood adaptation capacity. The map illustrates enhanced resilience strategies to address potential future compound flooding loss, including 2035 planned urban green areas (pink), suggested new urban green areas (red), and suggested riverbank enhancements (blue).

5. Discussion

Despite the trillions of dollars in assets located in coastal flood-prone delta areas (Aerts et al., 2014), investments in flood protection have often been insufficient (Jiang et al., 2018b). This is due to factors such as short-term economic considerations (de Ruig et al., 2019), a lack of consensus on the effectiveness of protection measures (Du et al., 2020), and concerns about making irreversible decisions that may become suboptimal over time (Aerts et al., 2014)). In fast-developing delta cities like Shanghai, rapidly urbanization causes future landscapes and infrastructure to change quickly, making effective flood control planning and decision-making increasingly difficult to predict. To help inform policy decisions, we have developed a detailed modeling approach to evaluate plausible flood management strategies. In this study, we present three measures of HSD, IGA, and LGS aimed at reducing flooding using a systematic model study and evaluation. We applied flood depth–damage curves to estimate potential loss of buildings and infrastructure at the census block level. A conceptual framework was proposed to define the roles of physical scientists, practitioners, and knowledge brokers to better inform decision-makers in managing flood risk for building resilient delta cities.

5.1 Increasing flood risks due to rapid urbanization of delta city

Cities in delta regions are particularly vulnerable to flood risks, including aggravated storm surges, fluvial flooding, and rainfall runoffs (Tessler et al., 2015; Jongman, 2018; Maymandi et al., 2022). Moreover, rapid urbanization deteriorates the ecosystem functions on flood mitigation (Chen et al., 2019; Wu et al., 2024). These challenges are significant obstacles to urbanizing deltas worldwide (Aerts et al., 2014; Dixon et al., 2006; Jongman, 2018; Tessler et al., 2015). Shanghai, situated in the Yangtze River Delta, is one of the world's largest estuarine delta cities and historically susceptible to compound flooding due to its low-lying topography and estuarine features (Balica et al., 2012; Hallegatte et al., 2013). Our study demonstrated the potential severe impact of the

Zhengzhou "7·20" rainstorm flood event in Shanghai under both single and compound flood risks. The rainstorm alone resulted in flooding over 219 km² (27% of the total area), causing an economic loss of $241 million. When combined with a storm surge, the flooded area expanded by 16% to 349 km², and economic losses increased by 1.3-fold to $546 million. This highlights the urgent need for enhanced adaption strategies to address the unique flooding challenges faced by Shanghai.

The establishment of the China Pilot Free Trade Zone in Shanghai in 2019 is expected to increase vulnerability to flood-related disasters due to rapid urbanization (Yin et al., 2019). Explosive economic growth will transform 68 km² of agricultural land into industrial and residential land by 2050. Consequently, assets exposed to single and compound flooding are projected to increase fourfold and eightfold by 2035 and 2050, respectively, with asset losses expected to rise twofold and fivefold due to continued urban development. The rapid GDP growth driven by urbanization in LGZ significantly amplifies the impacts of extreme flooding. The increase in impermeable surfaces, including the removal of vegetation and soil, contributes to the amplification of flooding, particularly for pluvial flood risks (Chen et al., 2019; Wang et al., 2020; Wu et al., 2024). The expansion of urban areas and impervious surfaces, especially in industrial and residential areas, further exacerbates flood losses (Wahl et al., 2015; Yang et al., 2022; Zhang et al., 2018). Given the anticipated rapid urbanization, comprehensive flood management strategies and the development of low-impact urban flood control facilities are essential for mitigating escalating flood risks in rapidly developing Shanghai and similar coastal cities.

5.2 Comparison of flood adaptation measures

Following traditional urban planning principles, flood control in developing delta cities typically relies on hard engineering solutions such as dikes to prevent river overflow, seawalls to block seawater overtopping, and drainage systems to manage rainfall-induced waterlogging (Sun et al., 2021). However, as in many cities, these large-scale engineering measures have been criticized because they are costly or may harm the environment (Du et al., 2020; Dunlop et al., 2023; van Slobbe et al., 2013). This research evaluated the hard engineering of HSD for fluvial and coastal flood prevention compare to the green engineering of IGA and LGS for pluvial flood prevention based on numerical simulations. Results indicate that raising dikes by 0.2~0.5 m effectively reduces flooding in large parts of the city. However, implementing HSD is challenging due to foundation stability issues and potential urban landscape disruption (Yi, 2018). Furthermore, HSD is less effective for pluvial flooding, necessitating regional pumps and sluice gate joint operations. In contrast, green engineering of LID measures present promising alternatives. While IGA may not provide the greatest reduction in asset exposure, it significantly benefits the ecological environment and sustainable city development. Moreover, by lowering the green area, LGS provides the greatest reduction in exposed assets and losses. However, either LGS or IGA does not prevent flood waters from entering the city and they alter the urban landscape and require strategic alignment with urban planning. These results highlight the importance of integrated adaptation strategies in urban planning to optimize compound flood resilience.

High investment costs can hinder the implementation of flood adaptation measures. According to dike construction standards (Du et al., 2020), raising the 992 km dike in LGZ by 0.5 m is estimated to cost $660 million in 2020. Assuming an annual maintenance cost of 1% of the initial cost, total costs of HSD by 2035 and 2050 will be approximately $759 million and $858 million, respectively. For IGA, using sponge city construction costs as a reference (Hu et al., 2019), the initial cost for the planned green area of 64 km² in LGZ is $500 million in 2020. Including maintenance, total costs by 2035 and 2050 will be $650 million and $750 million, respectively. LGS involves land excavation in addition to IGA. The construction cost for 1 m of LGS is $2 billion in 2020, with total costs by 2035 and 2050 reaching $2.2 billion and $2.5 billion, respectively, including maintenance. A comprehensive analysis reveals that while hard HSD strategies offer robust protection against coastal and fluvial flooding with immediate effect, LID strategies of IGA and LGS provide additional benefits in mitigating pluvial flooding and enhancing ecological resilience. Among these, LGS provides the most effective overall flood mitigation, while IGA has the best benefit/cost ratio, although they require significant land and has limited efficacy against coastal flooding. Managing compound flooding is complex and requires consideration of regional drainage systems, pumping, and underground pipelines. Therefore, a combination of drainage enhancement, green area expansion, and even deep tunnels is recommended (Hu et al., 2019). A cost-benefit analysis of these adaptation measures should be designed according to the specific flood risk characteristics of each city, which vary among coastal cities.

5.3 Implications for building resilient delta cities

Floods account for the largest portion of insured losses among global catastrophes (Aerts et al., 2014). Adopting integrated approaches to urban planning is essential to address both the immediate and long-term flooding challenges posed by climate change and rapid urbanization (Aerts et al., 2014; Du et al., 2020; de Ruig et al., 2019). The flooding challenges faced by Shanghai highlight the need for comprehensive flood management strategies that combine traditional engineering solutions with green infrastructure. We proved that building resilient cities must prioritize the integration of green infrastructure and LID solutions alongside traditional engineering methods. The methodology developed in this study is transferable to other delta cities and coastal communities worldwide, where flood resilience plans are under active discussion. The effective flood protection strategies often evolve through long-term, iterative processes (de Ruig et al., 2019; Du et al., 2020; Dunlop et al., 2023; Green et al., 2021). Notable examples include large-scale flood protection measures implemented in the Netherlands (van Slobbe et al., 2013), New Orleans, USA (Hallegatte, 2006), and the Wadden Sea region in Germany (Markus-Michalczyk, 2023), which have delivered significant economic and environmental benefits. These international cases provide valuable insights and inspiration for developing effective flood resilience policies in other vulnerable delta cities.

In order to better inform decision-makers about managing flood risks in vulnerable delta cities, collaboration is required among physical scientists, practitioners, and knowledge brokers to translate scientific knowledge into actionable strategies (Fig. 11). Physical scientists are responsible for generating and validating scientific knowledge about flood risks, including hydrological, meteorological, and geomorphological processes. Practitioners are on-the-ground professionals who implement strategies and manage infrastructure to reduce flood risk. Knowledge brokers act as intermediaries between scientists, practitioners, and decision-makers, ensuring that scientific findings are effectively communicated and integrated into policy and practice. For decision-makers to build resilient delta cities, *i)* physical scientists need to provide reliable, cutting-edge knowledge of flood risks and adaptation solutions; *ii)* practitioners have to apply this knowledge in designing and implementing practical measures; *iii)* knowledge brokers must ensure that the scientific and practical insights are communicated effectively, leading to informed and coordinated decisions. Together, these roles form a comprehensive approach to flood risk management, delta cities worldwide can better protect their populations, economies, and ecosystems from the adverse effects of climate change and urbanization.

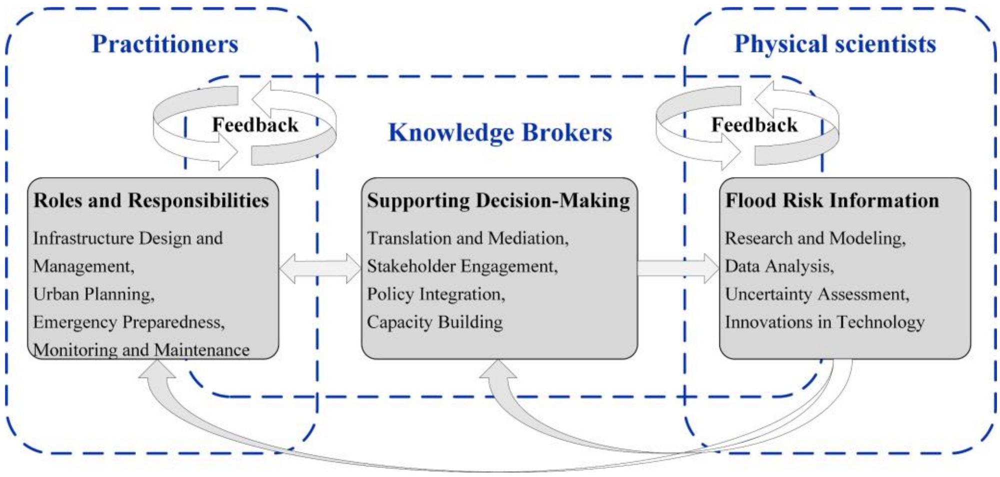

Fig. 11. A conceptual framework illustrating the role of knowledge brokers in connecting practitioners and physical scientists facilitating informed decision-making for building resilient delta cities.

5.4 Limitations and directions for future research

This study highlights how rapid urbanization and GDP growth drive land use changes that amplify flood risks in delta cities. However, the role of socio-economic dynamics should be assessed alongside critical hazard factors, such as long-term climate change, sea-level rise, and land subsidence, which are essential for future flood risk projections. While the high-resolution ocean-land coupled numerical model effectively simulates compound flood processes, its reliance on specific historical events, such as the Zhengzhou "7·20" rainstorm and Typhoon In-fa, may limit the generalizability of the findings to other delta cities with different hydrological and urban characteristics. Future research should explore integrated multi-scenario and multi-hazard frameworks, incorporating long-term climate projections, socio-economic dynamics, and diverse hazard return levels to enhance flood risk assessments. Additionally, expanding the model to include real-time flood forecasting with advanced machine learning techniques could enhance its applicability for rapid urban flood rescue and emergency management in other delta cities worldwide.

6. Conclusions

Rapid urbanization significantly increases flooding risks in delta cities such as Shanghai. This study evaluates flood risks and adaptation measures for LGZ, a rapidly developing estuary region, considering both current and future urbanization scenarios. High-resolution ocean-land coupled numerical model reveal that rapid urbanization exacerbates flooding risks, potentially increasing exposed assets and losses by up to eight and five times, respectively, by 2050. The transformation of land use from agricultural to industrial and residential areas results in more impermeable surfaces, intensifying pluvial flood risks. Business as a service industry is also expected to contribute significantly in future flood risks. To manage and mitigate the impact of rapid urbanization on urban flood risks, effective flood defense measures must be implemented, particularly concerning the future urban planning of industrial, residential, and business areas. The adaptation measure of HSD provides robust protection against fluvial and coastal flooding, though it faces challenges such as high costs and limited effectiveness against pluvial flooding. In addition, we proved that the implementation of green spaces, permeable surfaces, and LID solutions, such as IGA and LGS, can significantly reduce pluvial flooding. Our findings, consistent with recent studies on flood adaptation, advocate for the integration of gray and hybrid green-gray measures, emphasizing "infiltration" and "storage" functions to effectively mitigate waterlogging (Du et al., 2020; Hu et al., 2019; Sun et al., 2021). Overall, building resilient cities requires a comprehensive approach that addresses immediate flood risks while promoting long-term environmental sustainability (Aerts et al, 2014; Du et al., 2020; Hu et al., 2019; Liao, 2012). We recommend a combination of these measures, where applicable, to optimize flood resilience and promote sustainable development in rapidly urbanizing regions like LGZ. These findings offer valuable insights for developing flood-resilient cities in estuarine delta regions globally.

Acknowledgments

This research is supported by the National Natural Science Foundation of China (42171282) and Shanghai Pujiang Program (21PJC096).

References

Aerts, J. C. J. H., Botzen, W. J. W., Emanuel, K., et al. Evaluating Flood Resilience Strategies for Coastal Megacities[J]. Science, 2014, 344(6183), 473-475.

Balica, S.F., Wright, N.G., and Meulen, F. A flood vulnerability index for coastal cities and its use in assessing climate change impacts[J]. Nature Hazards, 2012, 64, 73-105.

Chen, S. Simulation analysis of Zhengzhou "7 · 20" extreme rainstorm Scenario in Shanghai urban area[J]. China Flood & Drought Management, 2022, 32 (09), 56-59+86. (in Chinese)

Chen, X.Y., Zhang, X.B., Church, J.A., et al. The increasing rate of global mean sea-level rise during 1993–2014[J]. Nature Climate Change, 2017, 7(7), 492-495.

Chen, Y., Xie, W., and Xu, X. Changes of Population, Built-up Land, and Cropland Exposure to Natural Hazards in China from 1995 to 2015[J]. International Journal of Disaster Risk Science, 2019, 10(4), 557-572.

Danish Hydraulic Institute (DHI). MIKE21 & MIKE3 Flow Model Advection-Dispersion Module Scientific Documentation[R]. DHI, 2016.

de Ruig, L.T., Barnard, P.L., Botzen, W.J.W., et al. An economic evaluation of adaptation pathways in coastal mega cities: An illustration for Los Angeles[J]. Science of The Total Environment, 2019, 678, 647-659.

DHI MIKE, 2011. 1 D-2 D Modelling – user manual. DHI water & environment.

Dixon, T.H., Amelung, F., Ferretti, A., et al. Space geodesy: Subsidence and flooding in New Orleans[J]. Nature, 2006, 441, 587-588.

Domingo, D., Palka, G., and Hersperger, A. M. Effect of zoning plans on urban land-use change: A multi-scenario simulation for supporting sustainable urban growth[J]. Sustainable Cities and Society, 2021, 6, 102833.

Du, S.Q., Scussolini, P., Ward, P.J., et al. Hard or soft flood adaptation? Advantages of a hybrid strategy for Shanghai[J]. Global Environmental Change, 2020, 61, 102037.

Dunlop, T., Glamore, W., and Felder, S. Restoring estuarine ecosystems using nature-based solutions: Towards an integrated eco-engineering design guideline[J]. Science of The Total Environment, 2023, 873, 162362.

Eitelberg, D.A., van Vliet, J., Verburg, P.H. A review of global potentially available cropland estimates and their consequences for model-based assessments[J]. Global Change Biology, 2015, 21, 1236–1248.

Fang, J., Lincke, D., Brown, S., et al. Coastal flood risks in China through the 21st century – An application of DIVA[J]. Science of The Total Environment, 2020, 704, 135311.

Guidelines for Flood Risk Mapping, 2017. People's Republic of China Water Industry Standard, ICS 13.060.10, P 58.

Green, D., O'Donnell, E., Johnson, M., et al. Green infrastructure: The future of urban flood risk management[J]? Wiley Interdisciplinary Reviews-Water, 2021, 8(6), e21560.

Hallegatte, S. A Cost-Benefit Analysis of the New Orleans Flood Protection System[J]. Regulatory Analysis, 2006, 06-02.

Hallegatte, S., Green, C., Nicholls, R. J., et al. Future flood losses in major coastal cities[J]. Nature Climate Change, 2013, 3(9), 802-806.

Hanson, S., Nicholls, R., Ranger, N., et al. A global ranking of port cities with high exposure to climate extremes[J]. Climatic Change, 2010, 104(1), 89-111.

Hasan, S.S., Zhen, L., Miah, Md.G., et al. Impact of land use change on ecosystem services: A review[J]. Environmental Development, 2020, 34, 100527.

Hu, H.Z., Tian, Z., Sun, L.X., et al. Synthesized trade-off analysis of flood control solutions under future deep uncertainty: An application to the central business district of Shanghai[J]. Water Research, 2019, 115067.

Hugo, G. Future demographic change and its interactions with migration and climate change[J]. Global Environmental Change, 2011, 21, 21-33.

Jiang, T., Zhao, J., Cao, L.G., et al. Projection of national and provincial economy under the shared socioeconomic pathways in China[J]. Climate Change Research, 2018a, 14 (01), 50-58.

Jiang, Y., Zevenbergen, C., and Ma, Y.C. Urban pluvial flooding and stormwater management: A contemporary review of China’s challenges and “sponge cities” strategy[J]. Environmental Science & Policy, 2018b, 80, 132-143.

Jiang, L., Yu, J., Wen, J.H., et al. Risk assessment of extreme flood in the north bank of the Hangzhou Bay under land use change scenarios[J]. Progress in Geography, 2021, 40(8), 1355-1370.

Jongman, B. Effective adaptation to rising flood risk[J]. Nature Communications, 2018, 9(1), 1986.

Kossin, J.P. A global slowdown of tropical-cyclone translation speed[J]. Nature, 2018, 558, 104-107.

Liao, G., He, P., Gao, X., et al. Land use optimization of rural production–living–ecological space at different scales based on the BP–ANN and CLUE–S models[J]. Ecological Indicators, 2022, 137, 15.

Liao, K.H. A Theory on Urban Resilience to Floods—A Basis for Alternative Planning Practices[J]. Ecology and Society, 2012, 17(4).

Lin, N., Emanueli, K. A., Smith, J. A., et al. Risk assessment of hurricane storm surge for New York City[J]. Journal of Geophysical Research: Atmospheres, 2010, 115(D18).

Maymandi, N., Hummel, M. A., and Zhang, Y. Compound coastal, fluvial, and pluvial flooding during historical hurricane events in the Sabine–Neches Estuary, Texas[J]. Water Resources Research, 2022, 58, e2022WR033144.

Markus-Michalczyk, H. Nature-Based Solutions for Flood Risk Reduction: North Sea Region, Flat Coasts and Estuaries[J]. SDGs in the European Region, 2023, 367-388.

Ministry of Emergency Management of the People’s Republic of China [EB/OL].

Nicholls, R.J., Lincke, D., Hinkel, J. et al. A global analysis of subsidence, relative sea-level change and coastal flood exposure[J]. Nature Climate Chang, 2021, 11, 338-342.

Rimal, B., Zhang, L., Keshtkar, H., et al. Quantifying the Spatiotemporal Pattern of Urban Expansion and Hazard and Risk Area Identification in the Kaski District of Nepal[J]. Land, 2018, 7(1), 37.

Shirzaei, M., and Bürgmann, R. Global climate change and local land subsidence exacerbate inundation risk to the San Francisco Bay Area[J]. Science Advance, 2018, 4(3).

Smith, P., Gregory, P.J., van Vuuren, D., et al. Competition for land[J]. Philosophical Transactions of the Royal Society B: Biological Sciences, 2010, 365(1554), 2941-2957.

SMBS, 2023. Shanghai Municipal Bureau of Statistics, https://tjj.sh.gov.cn/.

SMOB, 2021. Shanghai Municipal Oceanic Bureau, https://swj.sh.gov.cn/.

Stehfest, E., van Zeist, W.J., Valin, H., et al. Key determinants of global land-use projections[J]. Nature Communications, 2019, 10, 2166.

Sun, X.J., L, R.N., Shan, X.M., et al. Assessment of climate change impacts and urban flood management schemes in central Shanghai[J]. International Journal of Disaster Risk Reduction, 2021, 65,102563.

Syvitski, J. P. M., and Saito, Y. Morphodynamics of deltas under the influence of humans[J]. Global and Planetary Change, 2007, 57(3), 261-282.

Syvitski, J. P. M., Kettner, A. J., Overeem, I., et al. Sinking deltas due to human activities[J]. Nature Geoscience, 2009, 2(10), 681-686.

Tessler, Z.D., Vörösmarty, C.J., Grossberg, M., et al. Profiling risk and sustainability in coastal deltas of the world[J]. Science, 2015, 349(6248), 638-643.

Van, A.S., Verburg, P.H. Land cover change or land-use intensification: simulating land system change with a global-scale land change model[J]. Global Change Biology, 2013, 19, 3648-3667.

van Slobbe, E., de Vriend, H.J., Aarninkhof, S. et al. Building with Nature: in search of resilient storm surge protection strategies[J]. Natural Hazards, 2013, 65, 947-966.

Visser, H. and de Nijs, T. The Map Comparison Kit[J]. Environmental Modelling & Software, 2006, 21(3), 346-358.

Vitousek, S., Barnard, P., Fletcher, C. et al. Doubling of coastal flooding frequency within decades due to sea-level rise[J]. Scientific Reports, 2017, 7, 1399.

Vousdoukas, M.I., Mentaschi, L., Voukouvalas, E. et al. Global probabilistic projections of extreme sea levels show intensification of coastal flood hazard[J]. Nature Communications, 2018, 9, 2360.

Wang, F., Wang, X.T., Zhuang, L., et al. Analysis of flood situation in Futuan River Basin based on the transplantation of the "7·20" extreme rainstorm in Zhengzhou City[J]. China Flood & Drought Management, 2023, 33 (09), 19-24+55. (in Chinese)

Wahl, T., Jain, S., Bender, J., et al. Increasing risk of compound flooding from storm surge and rainfall for major US cities[J]. Nature Climate Change, 2015, 5(12), 1093-1097.

Wang, S.Y.S., Zhao, L., Yoon, J.H., et al. Quantitative attribution of climate effects on Hurricane Harvey's extreme rainfall in Texas[J]. Environmental Research Letters, 2018, 13(5).

Wang, L.Y., Zhang, M., Wen, J.H., et al. Simulation of extreme compound coastal flooding in Shanghai[J]. Advance in Water Science, 2019, 30 (04), 546-555. (in Chinese)

Wang, Y.B., Xie, X.H., Liang, S., et al. Quantifying the response of potential flooding risk to urban

growth in Beijing[J]. Science of The Total Environment, 2020, 705, 135868.
Woodruff, J., Irish, J., and Camargo, S. Coastal flooding by tropical cyclones and sea-level rise[J]. Nature, 2013, 504, 44-52.
Wolff, S., Schrammeijer, E.A., Schulp, C.J.E., et al. Meeting global land restoration and protection targets: What would the world look like in 2050[J]? Global Environmental Change, 2018, 52, 259-272.
Wu, S.P., Zhou, X.D., Reyns, J., et al. Climate change and urban sprawl: Unveiling the escalating flood risks in river deltas with a deep dive into the GBM river delta[J]. Science of The Total Environment, 2024, 947, 174703.
Yang, K.X., Hou, H., Li, Y., et al. Future urban waterlogging simulation based on LULC forecast model: A case study in Haining City, China[J]. Sustainable Cities and Society, 2022, 87, 104167.
Yamamoto, T., Kazama, S., Touge, Y., et al. Evaluation of flood damage reduction throughout Japan from adaptation measures taken under a range of emissions mitigation scenarios[J]. Climatic Change, 2021, 165, 60.
Yi, S. Risk assessment and adaptive strategy of the compound scenarios of sea level rise and the probable maximum storm surge: A case study of Shanghai[D]. East China Normal University, 2018. (in Chinese)
Yin, J., Yin, Z., Yu, D.P., et al. Vulnerability Analysis for Storm Induced Flood: A Case Study of Huangpu River Basin[J]. Scientia Geographica Sinic, 2012, 32(09), 1155-1160. (in Chinese)
Yin, J., Zhao, Q., Yu, D.P., et al. Long-term flood-hazard modeling for coastal areas using InSAR measurements and a hydrodynamic model: The case study of Lingang New City, Shanghai[J]. Journal of Hydrology, 2019, 571, 593-604.
ZBNRP, 2023. Zhengzhou Bureau of Natural Resources and Planning, https://zrzyhghj.zhengzhou.gov.cn/.
Zhang, W., Villarini, G., Vecchi, G.A., et al. Urbanization exacerbated the rainfall and flooding caused by hurricane Harvey in Houston[J]. Nature, 2018, 563(7731), 384-388.